Journal of Catalysis **198,** 66–76 (2001)
doi:10.1006/jcat.2000.3126, available online at http://www.idealibrary.com on IDEAL®

Thermal Decomposition of Dimethyl Methylphosphonate over Manganese Oxide Catalysts

Scott R. Segal,* Lixin Cao,* Steven L. Suib,*,†,‡,[1] Xia Tang,§ and Sunita Satyapal§

*U-60, Department of Chemistry, †Department of Chemical Engineering, and ‡Institute of Materials Science, University of Connecticut, Storrs, Connecticut 06269-3060; and §United Technologies Research Center, 411 Silver Lane, East Hartford, Connecticut 06108

Received July 17, 2000; revised October 30, 2000; accepted November 28, 2000; published online February 7, 2001

The thermal oxidative decomposition of dimethyl methylphosphonate (DMMP) has been studied over amorphous manganese oxide (AMO) and Al_2O_3-supported manganese oxide catalysts. The reaction was carried out using air as the oxidant at temperatures between 200 and 400°C. The highest reaction rates occurred using temperatures of 400°C. Gas chromatography (GC) was used to examine reactant DMMP and other gas phase products. DMMP was found to oxidatively decompose over AMO and Al_2O_3-supported manganese oxide catalysts. The highest activity was observed using a catalyst prepared by precipitation of AMO on Al_2O_3. During the initial stages of reaction, DMMP was completely removed from the gas phase. During this period DMMP was oxidized to CO_2, with no other gas phase products being observed. After a certain period of time (5 min–8 h), DMMP reappeared in the gas phase. The CO_2 concentration then decreased and MeOH began to form, indicative of hydrolysis of DMMP. These results indicate that deactivation of catalysts occurs due to adsorbed P-species. Fourier transform infrared (FTIR) spectroscopy and ion chromatography (IC) were used to examine adsorbed products on the surface of the catalysts. The IC analyses indicated that several products accumulate on the surface of the catalysts, including methyl methylphosphonate, methylphosphonic acid, and phosphoric acid. FTIR analyses showed that DMMP bonds strongly to Mn Lewis acid sites on the manganese oxide surface via phosphoryl oxygen. The bare Al_2O_3 support was also examined in DMMP decomposition reactions and showed high activity, with 100% DMMP removal from the gas stream for over 15 h. The major products observed over Al_2O_3 were dimethyl ether and MeOH. No CO_2 was observed, indicating that DMMP is not oxidized over Al_2O_3. The GC, IC, and FTIR results suggest that DMMP is dissociatively adsorbed over Al_2O_3. Finally, the results for the thermal oxidation of DMMP over AMO are compared to results previously obtained using photo-assisted oxidative methods.

I. INTRODUCTION

The decomposition of organophosphorous compounds continues to be of interest, due to the need for safe removal of chemical warfare agents (CWAs). In the United States alone, there are approximately 25,000 tons of chemical weapons stockpiled (1). In order to reduce these stockpiles safely, the development of methods alternate to incineration is desired. Dimethyl methylphosphate (DMMP), whose structure is shown in Fig. 1, is a widely used simulant for CWAs and other toxic organophosphorous compounds such as pesticides.

In our previous paper we have investigated the oxidative photo-assisted decomposition of DMMP over mixed valent, amorphous manganese oxide (AMO) catalysts (2). This work showed that under dark conditions (25°C), DMMP strongly absorbs to the AMO surface. After irradiation with UV-vis light, several gas phase products were formed. These products included methanol and CO_2. After a brief period of high activity, the amounts of the products decreased significantly as the catalyst surface became poisoned by adsorbed phosphorous species. The spent catalysts were extracted in H_2O and the extracts were analyzed by ion chromatography (IC). These results showed that several products accumulate on the AMO surface, including methyl methylphosphonate (MMP) and methyl phosphonic acid (MPA). Additionally, adsorbed DMMP was found on the surface. Under these conditions no phosphoric acid was detected, which indicated the incomplete decomposition of DMMP, MMP, and MPA. Fourier transform infrared (FTIR) spectroscopy was also used to examine the nature of the adsorbed species on the catalysts. These results confirmed the findings from the IC data.

The thermal decomposition of DMMP has been studied over metals, including Mo(111) (3), Pt(111) (4), Pd(111) (5), and Ni(111) (5), and metal oxides such as Fe_2O_3 (6), MgO (7–9), La_2O_3 (10), Pt/Al_2O_3 (11), Fe_2O_3/Al_2O_3 (12), $Fe_2O_3/CaO/MgO$ (13), V_2O_3/MgO (13), and Cu-substituted hydroxyapatite (14). We have recently found some very active catalysts for DMMP decomposition based on V_xO_y supported on Al_2O_3 and SiO_2 (15). These catalysts showed exceptionally high activity because they caused the formation of P_2O_5, which itself proved to be catalytically active for further decomposition of DMMP. One of the main issues

[1] To whom correspondence should be addressed.

0021-9517/01 $35.00

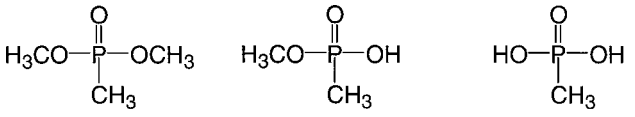

FIG. 1. Structures of dimethyl methylphosphonate (DMMP), methyl methylphosphonate (MMP), and methylphosphonic acid (MPA).

that plagues catalytic (photo and thermal) oxidation studies of DMMP is catalyst poisoning due to adsorbed phosphorous species. Therefore, the sustained oxidative catalysis of DMMP over metals and metal oxides is difficult to attain unless temperatures of greater than 600°C are used (3).

In this work we have continued our investigation on the decomposition of DMMP over manganese oxide catalysts. The thermal oxidative decomposition of DMMP was studied over AMO catalysts between 200 and 400°C using air as the oxidant. Additionally, several Al_2O_3-supported manganese oxide samples were prepared, characterized, and tested in thermal oxidative DMMP decomposition reactions. After DMMP reactions, the catalysts were examined using FTIR and IC to assist in identifying products and for determining decomposition mechanisms.

II. EXPERIMENTAL

A. Preparation of materials. AMO was prepared by a redox reaction involving the reduction of $KMnO_4$ with oxalic acid. A solution containing 1.58 g of $KMnO_4$ (Aldrich, Milwaukee, WI) in 100 mL of distilled deionized water (DDW) was mixed with a solution containing 2.26 g of oxalic acid (Fisher, Fair Lawn, NJ) in 100 mL of DDW. The solution was allowed to mix for several hours, which then yielded a dark brownish–black precipitate. The solid was filtered and washed with DDW several times and then dried in an oven at 110°C overnight. A portion of the sample was calcined in air at 400°C for 4 h.

Two different Al_2O_3-supported manganese oxide samples were prepared. The first sample was synthesized by precipitation of AMO on γ-Al_2O_3. This was made by slowly adding solutions of $KMnO_4$ (1.58 g in 25 mL of DDW) and oxalic acid (2.26 g in 25 mL of DDW) to a slurry containing 5.0 g of γ-Al_2O_3 (Davison, Chattanooga, TN) in 50 mL of DDW. The mixture was stirred for 18 h, which yielded a light-brown solid. The mixture was heated on a stir plate at ~60°C for 4 h. The sample was then placed in an oven and heated in air for 18 h at 120°C. Finally, the light-brown solid was calcined in air at 400°C for 4 h. This sample will be hereafter designated AMO/Al_2O_3.

The second Al_2O_3-supported manganese oxide sample was prepared by wet impregnation of $Mn(NO_3)_2 \cdot 6H_2O$ onto γ-Al_2O_3. A Mn^{2+} solution was prepared by dissolving 1.16 g of $Mn(NO_3)_2 \cdot 6H_2O$ (Aldrich) in 100 mL of DDW. To this solution, 2.0 g of γ-Al_2O_3 was added and the solution was stirred overnight. The next day, a dark brown–black solid was observed. The sample was heated slowly for several hours on a heating plate and then was placed in an oven and dried in air at 120°C for 18 h. The final black product was calcined at 400°C for 4 h. This sample will be hereafter designated Mn/Al_2O_3.

B. Catalytic studies. DMMP was purchased from Aldrich and was used without further purification. A schematic diagram of the reactor used for thermal DMMP decomposition reactions is shown in Fig. 2. Air was used in as the oxidant and was passed through a bubbler containing liquid DMMP, which was kept in a water bath at 25°C. The flow rate of air was kept between 30 and 50 mL/min. The DMMP-saturated air was then passed through a glass tube (ID = 1/4″) containing either 50 or 100 mg of the catalyst which was packed between glass wool plugs. Under these conditions, the inlet DMMP concentration is ~0.14 mol%. The outlet lines (after the furnace) were heated to 120°C to prevent condensation of DMMP and other products. Prior to the DMMP decomposition reactions, the catalysts were heated for 30 min in air at the temperature used in the particular experiment.

C. GC analyses. Reactants and products were analyzed using a Hewlett–Packard 5890 Series I gas chromatograph equipped with an automatic gas-sampling valve. A Carbowax 20M capillary column with flame ionization detection was used to analyze for DMMP, methanol (MeOH), and dimethyl ether (DME). CO_2 was analyzed using a GSC Gas Pro capillary column with thermal conductivity detection. Calibration curves for MeOH, DME, and CO_2 were prepared from gas standards prepared in our laboratories.

D. X-ray diffraction analyses. A Scintag Model PDS-2000 θ-θ diffractometer was used for X-ray powder diffraction (XRD) experiments. Cu $K\alpha$ radiation was used at 45 kV and 40 mA. Sample scans were done at 5°2θ/min.

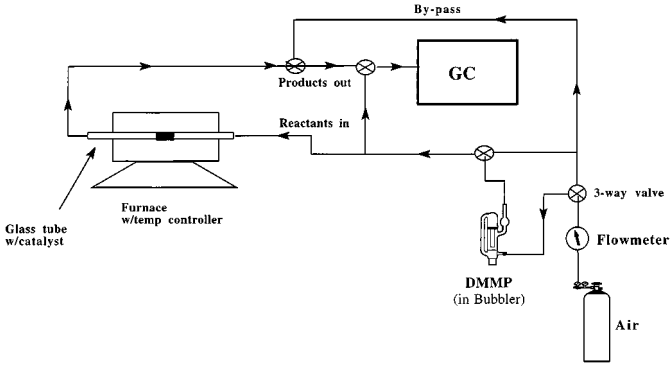

FIG. 2. Experimental setup used for thermal DMMP decomposition reactions.

E. Inductively coupled plasma (ICP) analyses. The manganese concentrations in the catalysts were measured using a Perkin–Elmer P40 ICP Analyzer. Prior to analysis, the samples were dissolved in a small amount of HF and were then diluted with distilled deionized water. Several milliliters of HCl were added to assist in dissolving the manganese.

F. FTIR analysis. Fourier transform infrared spectroscopy (Nicolet Magna-IR 750) was used to examine surface species on the catalysts after DMMP reactions. A DTGS detector with a KBr beam splitter was used for analysis over the entire mid-IR range (4000–400 cm^{-1}). The samples were pressed into KBr pellets (2.5% sample by weight), and transmission spectra were collected.

G. Extraction analyses of spent AMO. Aqueous extractions of AMO after DMMP reactions were used to identify methylphosphonic acid, methyl methylphosphonate, and phosphates (PO_4^{3-}). The structures of MPA and MMP are shown along with DMMP in Fig. 1. The aqueous extracts were prepared by placing the spent AMO in H_2O and treating it with ultrasound for 10 min. The solution was filtered through 0.22-μm filters and analyzed using a Dionex DX 500 ion chromatograph equipped with a CD 20 conductivity detector and a Dionex AS4A-SC anion exchange column. The eluent used was 1.8 mM Na_2CO_3/1.7 mM $NaHCO_3$ buffer (app. pH 10).

In order to confirm the presence of MPA and MMP in the IC analyses, standards were prepared and retention times were established. MPA was available commercially (Aldrich), whereas MMP needed to be synthesized in our laboratories. MMP was prepared according to literature procedures by partial hydrolysis of DMMP in aqueous NaOH solution (16). In this procedure, 0.140 mol DMMP was added to 150 mL of a 10% NaOH solution and refluxed gently for 5 h. The solution was cooled slowly and acidified to pH 2 with concentrated HCl. The solution was vacuum distilled until a NaCl precipitate was observed in the distillation flask. The mixture was extracted several times with acetone and then filtered. The acetone extract was dried over $CaSO_4$ for several hours. The extract was refiltered and placed in a rotovap until ~15–20 mL of liquid remained. The sample was vacuum distilled and a distillate was collected almost immediately. This distillation was necessary to remove trace amounts of acetone in the mixture. Following several more minutes of distillation, a small amount of liquid (~1 mL) was observed in the receiving flask. The liquid was identified as MMP and was confirmed by ^1H NMR studies (17).

III. RESULTS

A. AMO preparation. AMO is formed through the reduction of $KMnO_4$ by oxalic acid. From previous work we have shown that, after drying, the composition of AMO is $K_{0.6}Mn_{0.93}O_2$ (18). AMO has an average Mn oxidation state of 3.5–3.6 (18), which indicates that AMO is a mixed valent manganese oxide. The XRD patterns for AMO and calcined AMO are shown in Fig. 3. These data show that AMO is not entirely amorphous, as a few small and broad peaks are seen. These include two peaks with d-spacings of 6.92 and 2.42 Å. A portion of the AMO material was calcined at 400°C for 4 h. The XRD pattern for calcined AMO shows that many new peaks are formed, indicating that the material becomes crystalline during heating. In the calcined AMO sample, peaks appear at 6.87, 4.86, 3.46, 3.10, 2.45, 2.38, 2.30, 2.19, 2.15, 1.92, 1.82, 1.63, and 1.54 Å. The labels written on the XRD patterns denote phases and will be discussed in later sections. The broad peaks occurring between ~15 and 25°2θ are due to SiO_2 (microscope slides), used to support the powder samples.

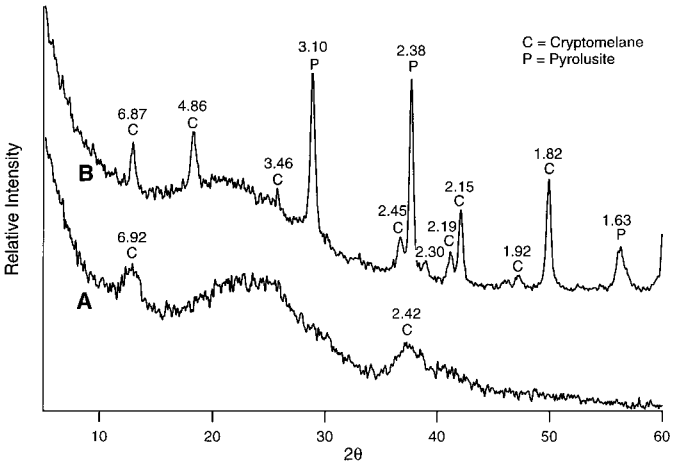

FIG. 3. Powder X-ray diffraction patterns for (A) AMO and (B) AMO calcined at 400°C for 4 h.

B. AMO/Al_2O_3. After the $KMnO_4$ solution is mixed with the oxalic acid solution in the presence of Al_2O_3, vigorous bubbling is observed, similar to that observed with unsupported AMO syntheses. However, the color of the AMO/Al_2O_3 sample is very different than that of unsupported AMO. Unsupported AMO is essentially black, while AMO/Al_2O_3 is light brown (even after calcination). ICP analysis reveals that AMO/Al_2O_3 contains 6.18% Mn by weight. The XRD pattern for calcined AMO/Al_2O_3 is shown in Fig. 4. The XRD pattern shows a few broad peaks centered at 2.39 and 1.96 Å.

C. Mn/Al_2O_3. Impregnation of the manganese(II) nitrate solution over Al_2O_3 results in the formation a black solid. After calcination, ICP analysis reveals that the sample contains 6.52% Mn by weight. The X-ray pattern for calcined Mn/Al_2O_3 is shown in Fig. 5. This shows the formation of several peaks, with d-spacings of 3.11, 2.41, 2.11, 1.97, 1.62, and 1.56 Å.

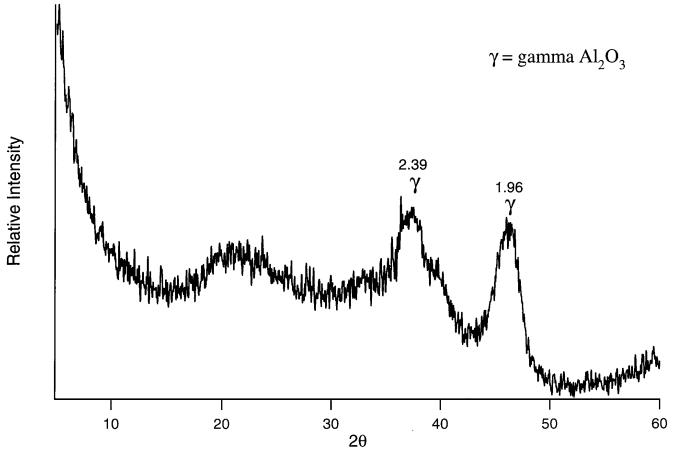

FIG. 4. Powder X-ray diffraction patterns for AMO/Al_2O_3 calcined at 400°C for 4 h.

D. Thermal DMMP decomposition reactions over AMO. It should first be noted that, in the absence of catalysts, no measurable DMMP decomposition is observed at temperatures up to 400°C. In initial experiments, we examined the decomposition of DMMP over unsupported AMO at temperatures between 200 and 400°C. Plots showing the fate of DMMP and formation of products are shown in Fig. 6. In Fig. 6A, the data points seen on the left *y*-axis represent the initial DMMP concentration, which is between 0.13 and 0.14 mol%. These data show initially that at all temperatures DMMP is completely removed from the gas stream. After a period of time, DMMP begins to reappear in the gas stream. This period of time when 100% DMMP decomposition occurs, typically toward the beginning of DMMP decomposition reactions, is often referred to as "protection time" (14). These data show that the protection time for DMMP decomposition reactions increases with temperature. At 200°C, DMMP is only completely removed from the gas stream for a few minutes. At 300°C, the protection time increases to ~30 min, while at 400°C the protection time is almost 1 h.

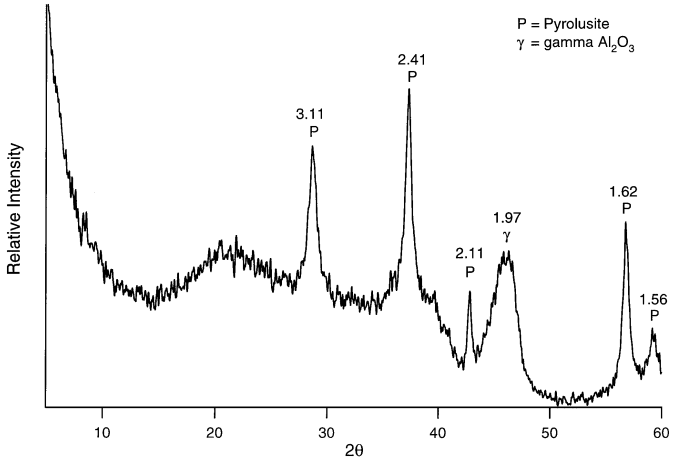

FIG. 5. Powder X-ray diffraction patterns for Mn/Al_2O_3 calcined at 400°C for 4 h.

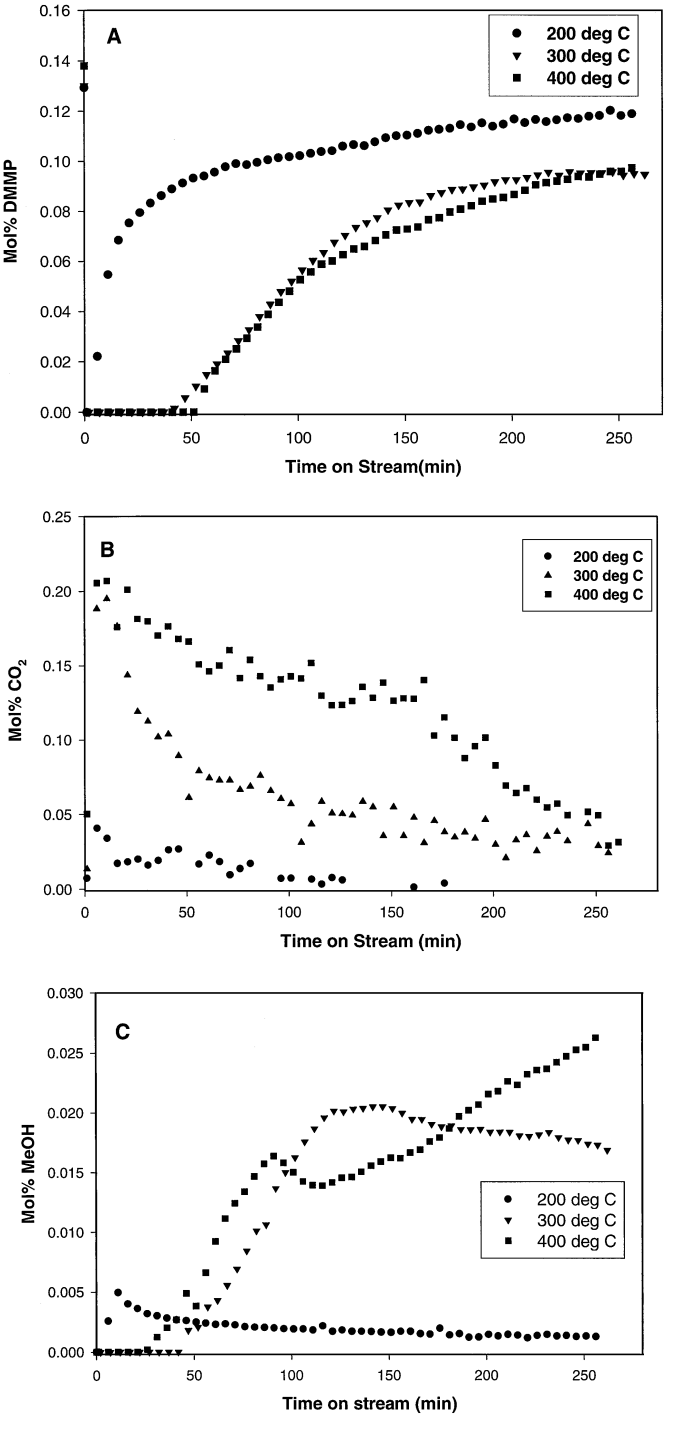

FIG. 6. Profile showing (A) fate of DMMP and formation of (B) CO_2 and (C) MeOH as a function of time over AMO at different temperatures. Reaction conditions: 50 mg AMO, air flow rate = 30 mL/min.

The gas stream products that were detected included CO_2 and MeOH. In Figs. 6B and 6C, the profiles for CO_2 and

MeOH are shown at the different temperatures used in the DMMP decomposition reactions. The profile for CO_2 production shown in Fig. 6B indicates that large amounts of CO_2 are produced at 300 and 400°C, especially toward the beginning of the reactions. At these temperatures the initial concentrations of CO_2 are around 0.20 mol%. The concentration of CO_2 then begins to decrease as a function of reaction time. At 200°C, only low levels of CO_2 (~0.05 mol%) are observed toward the beginning of the reactions. After approximately 2 h, no CO_2 is detected at this temperature.

The MeOH profiles for DMMP decomposition over AMO are shown in Fig. 6C. At 300 and 400°C, no MeOH is initially detected. After 30–45 min MeOH appears in the gas stream, and its concentration for the most part increases with time. At 300°C, the MeOH concentration reaches a maximum at 0.020 mol% after 140 min. The MeOH concentration then begins to slowly decrease. This trend is different than that observed at 400°C. At 400°C, the MeOH concentration essentially increases with time. At 200°C, the profile for MeOH looks quite different than that observed with higher temperatures. Initially, the MeOH concentration is zero and quickly reaches a maximum at 0.005 mol% after only about 15 min. The MeOH concentration then decreases slowly with time.

In another set of experiments, the decomposition of DMMP was studied over AMO at 400°C using slightly different conditions. In these experiments, the flow rate of air was increased from 30 to 50 mL/min. Also, the amount of catalyst was doubled from 50 to 100 mg. These changes in the reaction conditions were found to cause a slight difference in the catalytic results. In Fig. 7, the profiles for DMMP, MeOH, and CO_2 are shown for a DMMP decomposition reaction over AMO using these new conditions. The main difference in these results compared to results obtained in previous experiments is that the protection time has decreased from 1 h to only several minutes. The trends for MeOH and CO_2 production are similar to results obtained in previous experiments; however, the MeOH concentration is slightly lower in these experiments.

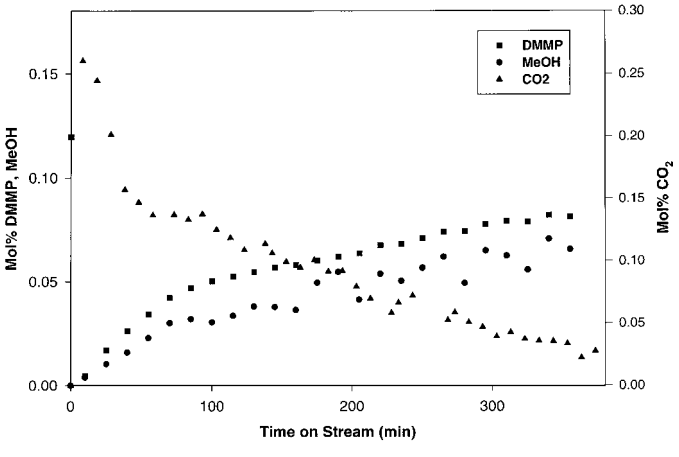

FIG. 7. Profile showing fate of DMMP and the formation of products in thermal DMMP decomposition reactions over AMO at 400°C. Reaction conditions: 100 mg AMO, air flow rate = 50 mL/min. $T = 400$°C.

E. Thermal DMMP decomposition reactions over Al_2O_3 and Al_2O_3-supported manganese oxides. A systematic study of DMMP decomposition reactions over Al_2O_3 and Al_2O_3-supported manganese oxide materials was carried out at 400°C. The results for these experiments are shown in Fig. 8. The results shown in Fig. 8A indicate that γ-Al_2O_3 is quite active in DMMP decomposition reactions. Some major differences are observed compared with AMO catalysts. The most significant observation is the length of time in which DMMP is completely removed from the gas stream. The protection time for Al_2O_3 is over 15 h. In contrast to reactions using AMO as the catalyst, no CO_2 is formed in this reaction. However, another product is observed throughout the reaction, which was identified as dimethyl ether. MeOH is also formed in this reaction, starting after 10 h. The concentration of MeOH increases rapidly to almost 0.08 mol% after around 20 h.

In Fig. 8B the results for the DMMP decomposition reaction over AMO/Al_2O_3 at 400°C are shown. The protection time is just over 8 h, followed by a slow increase in the DMMP concentration. In contrast to results obtained using unsupported Al_2O_3, CO_2 is produced in DMMP decomposition reactions over AMO/Al_2O_3. The initial CO_2 concentration is ~0.21 mol%. As with AMO samples, the CO_2 concentration then decreases as a function of reaction time. Although not shown in the plot, a trace amount of DME was also observed throughout the reaction. The formation of MeOH begins to occur starting after 7.5 h. The MeOH concentration then continues to increase as a function of time.

In Fig. 8C, the results for the DMMP decomposition reaction over Mn/Al_2O_3 are shown. These results are similar to those observed using AMO/Al_2O_3. The one difference here is that the protection time is somewhat shorter (~4 h). Generally the same types and amounts of products are formed in this reaction compared with the AMO/Al_2O_3 sample. Once again, trace amounts of DME were observed throughout the entire reaction.

F. IR analyses. IR analyses were used to examine adsorbed phosphorous species on the catalysts after DMMP reactions. In order to identify these species, the IR data for liquid DMMP were collected and the frequencies and assignments are listed in Table 1. The spectrum was measured by placing a small drop of DMMP onto a KBr pellet. Note that there are two important regions of the IR spectrum that are important for DMMP analysis. This includes a high-frequency region between 3200 and 2600 cm^{-1} and a low-frequency region between 1800 and 750 cm^{-1}. The higher frequency region contains peaks caused by methyl group stretching, while the lower frequency region contains peaks caused by C–O, C–P, and P=O stretching vibrations

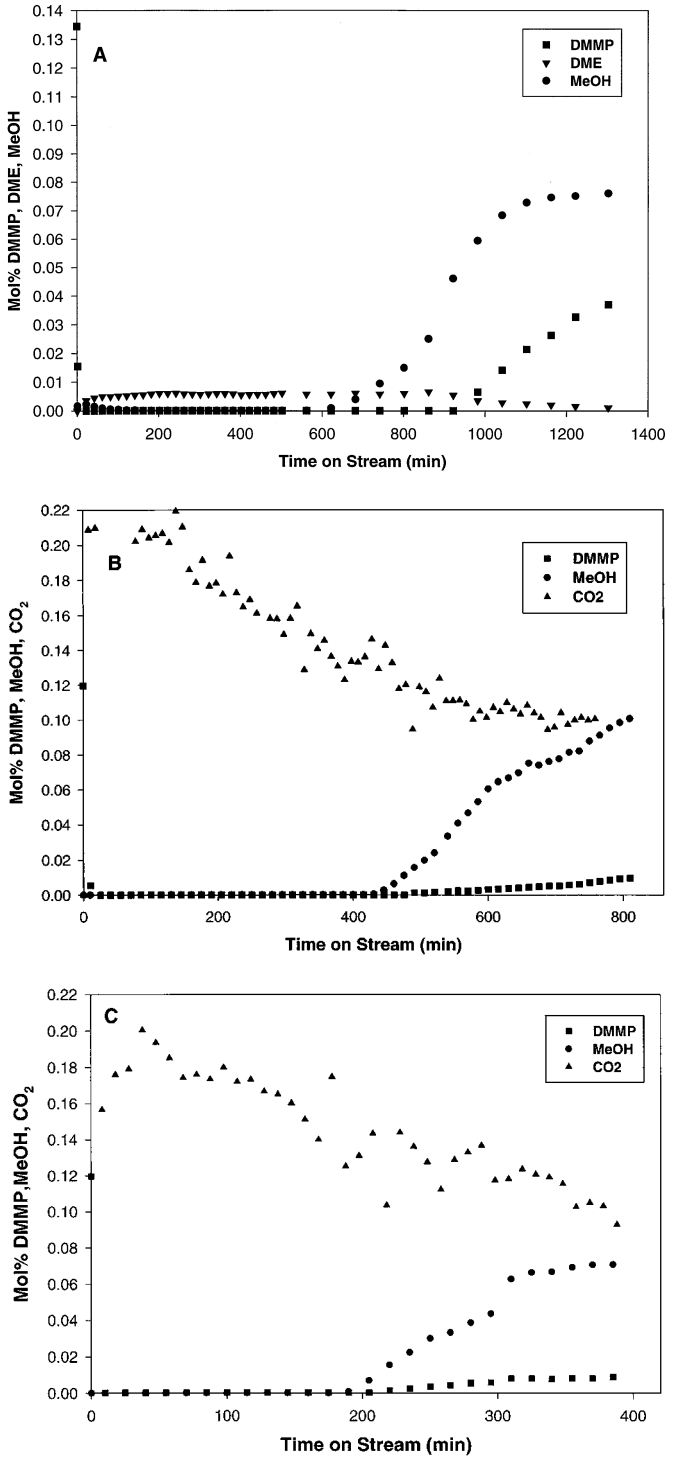

FIG. 8. Profile showing fate of DMMP and the Formation of Products in Thermal DMMP decomposition reactions over (A) γ-Al_2O_3, (B) AMO/Al_2O_3, and (C) Mn/Al_2O_3 at 400°C. Reaction conditions: 100 mg catalyst, air flow rate = 50 mL/min. $T = 400$°C.

as well as methyl deformation vibrations (10). The IR spectra for all catalysts before and after DMMP decomposition reactions at 400°C were measured and are shown in Fig. 9. The IR data are summarized in Table 2.

TABLE 1

IR Frequencies and Assignments for DMMP

Vibrational mode[a]	Frequency (cm^{-1})
ν_a (CH_3P)	2997
ν_a (CH_3O)	2956
ν_s (CH_3P)	2930
ν_s (CH_3O)	2854
δ_s (CH_3P)	1317
ν (P=O)	1250
ρ (CH_3O)	1189
ν (CO)	1062
ν (CO)	1036
ρ (CH_3P)	914
ν (PO_2)	820
ν (PO_2)	789
ν (PC)	711

Note. ν, stretch; δ, deformation; ρ, rock; a, antisymmetric; s, symmetric.

[a] Values for vibrational modes are taken from Ref. (10).

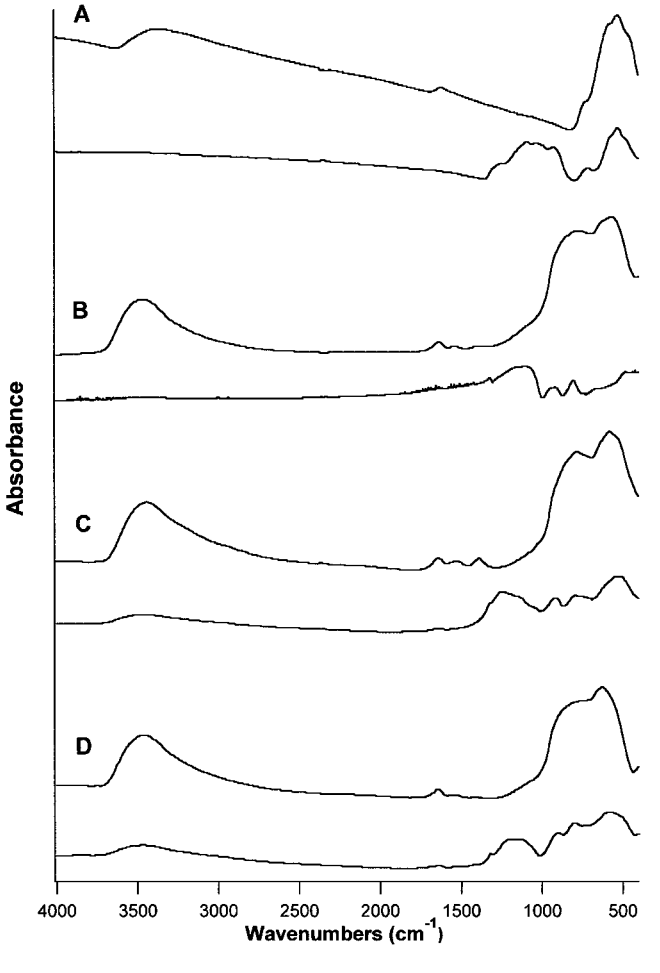

FIG. 9. IR spectra of (A) AMO before and after 6.5 h of DMMP rxn, (B) γ-Al_2O_3 before and after 23 h of DMMP rxn, (C) AMO/Al_2O_3 before and after 13.5 h, and (D) Mn/Al_2O_3 before and after 7 h of DMMP rxn. $T = 400$°C. Note that in each series, the top spectrum is before rxn and lower spectrum is after rxn.

TABLE 2

Summary of IR Data for Catalysts before and after Thermal DMMP Decomposition Reactions at 400°C

Sample	Freq (cm^{-1})	Vib mode[a]	Sample	Freq (cm^{-1})	Vib mode
AMO (before rxn)	3300	ν (OH)	AMO/Al_2O_3 (before rxn)	3444	ν (OH)
	1622	ν (H_2O)		1638	ν (H_2O)
	500	ν (Mn–O)		1531	ν (H_2O)
				1386	ν (H_2O)
AMO (after rxn)	1238	ν (P=O)		779	ν (Al–O)
	1088	ν (PO_3)		578	ν (Al–O, Mn–O)
	1029	ν (PO_2)			
	925	ν (CH_3P)			
	711	ν (PC)	AMO/Al_2O_3 (after rxn)	3451	ν (OH)
				1639	ν (H_2O)
γ-Al_2O_3 (before rxn)	3470	ν (OH)		1242	ν (P=O)
	1636	ν (H_2O)		1150	ν (PO_3)
	1540	ν (H_2O)		916	ρ (PCH_3)
	1368	ν (H_2O)		792	ν (PO_2)
	762	ν (Al–O)		524	ν (Al–O, Mn–O)
	572	ν (Al–O)			
			Mn/Al_2O_3 (before rxn)	3459	ν (OH)
γ-Al_2O_3 (after rxn)	3447	ν (OH)		1638	ν (H_2O)
	3001	ν_a (CH_3P)		778	ν (Al–O)
	2935	ν_s (CH_3P)		619	ν (Al–O, Mn–O)
	1321	δ (CH_3P)			
	1165	ν (P=O)	Mn/Al_2O_3 (after rxn)	3459	ν (OH)
	1108	ν (PO_2)		1650	ν (H_2O)
	918	ρ (CH_3P)		1419	ν (CH_3P)
	802	ν (PO_2)		1321	δ (PCH_3)
	668	ν (Al–O)		1204	ν (P=O)
	477	ν (Al–O)		1138	ν (PO_3)
				901	ρ (CH_3P)
				800	ν (PO_2)
				584	ν (Al–O, Mn–O)

[a] Values for vibrational modes are taken from Ref. (10). ν, stretch; δ, deformation; ρ, rock; a, antisymmetric; s, symmetric.

G. Extraction analyses of spent catalysts. The results of the IC analyses for extractions made on the catalysts after thermal reactions are listed in Table 3. Quantitative data for MMP could not be obtained for these experiments because the MMP standard had reacted over time (converted to MPA). Therefore, MMP was only qualitatively analyzed. Some problems were observed in these studies due to the presence of silica fibers from the glass wool used during the thermal decomposition reactions. Therefore, errors are likely in these data.

TABLE 3

Ion Chromatography (IC) Data for Catalysts after DMMP Decomposition Reactions at 400°C

Sample	PO_4^{3-}	MPA (mg/g)	MMP
Al_2O_3 (after 23 h)	2.48	140.8	Trace
AMO (after 6 h)	21.04	1.19	Trace
AMO/Al_2O_3 (after 13.5 h)	13.17	30.52	Some
Mn/Al_2O_3 (after 6.4 h)	2.13	60.90	Some

The IC data for thermal DMMP decomposition reactions over manganese oxides show some major differences compared to results obtained for photoreactions. The most important observation for catalysts after thermal reactions is the formation of PO_4^{3-}, especially when using AMO and AMO/Al_2O_3. The formation of PO_4^{3-} was not observed during photoreactions of DMMP over AMO (2). Small amounts of PO_4^{3-} were also observed using γ-Al_2O_3; however, the major product accumulated on the catalyst is MPA (140.8 mg/g). For manganese-oxide-supported Al_2O_3 catalysts, PO_4^{3-} is observed in both samples, with the AMO/Al_2O_3 catalyst having a greater amount of accumulated PO_4^{3-} (13.17 vs 2.13 mg/g). MMP was observed on all catalysts after thermal DMMP decomposition reactions.

H. Turnover numbers (TON) for thermal DMMP decomposition reactions. In order to get an idea whether thermal DMMP decomposition reactions occur stoichiometrically or catalytically over manganese oxide materials, TONs were calculated for all of the catalysts. The results of these calculations are given in Table 4. For comparison, the TON for DMMP photoreactions over AMO is also

TABLE 4

Turnover Numbers (TON) for Catalysts in DMMP Decomposition Reactions

Sample	TON[a]
AMO (photoreaction)	0.0529
AMO (400°C)	0.179
AMO/Al_2O_3 (400°C)	1.22
Mn/Al_2O_3 (400°C)	1.87
Al_2O_3 (400°C)[b]	0.0458

[a] TON is defined as (total mol products)/(mol Mn)(h).
[b] Mol Al substituted for mol Mn.

included. More will be said about these numbers in the Discussion.

IV. DISCUSSION

A. Catalyst preparation and characterization. The average Mn oxidation state of 3.5–3.6 in AMO suggests that Mn exists in mixed valencies, most likely a mixture of 3^+ and 4^+, with some 2^+ (18). Mixed valency is an important property for redox catalysis and commonly occurs with manganese oxide materials (19). Another property of AMO that contributes to its applications in catalysis and adsorption is its high surface area. BET surface area measurements indicate that AMO has a surface area of 200 m^2/g (20).

The X-ray diffraction data shown in Fig. 3 indicate that uncalcined AMO has some crystallinity. The peaks at 6.92 and 2.42 Å match the two strongest peaks in the JCPDS pattern for the mineral cryptomelane. Cryptomelane belongs to a family of porous, mixed valent manganese oxides known as octahedral molecular sieves. These materials consist of edge- and corner-sharing MnO_6 octahedra that have tunnels on the order of molecular dimensions (21). The composition of cryptomelane is known to be $KMn_8O_{16} \cdot nH_2O$, which is reasonably close to the composition we determined for AMO (21). After calcination the XRD pattern indicates that AMO crystallizes further as pyrolusite, a MnO_2 phase is formed. This suggests that AMO is further oxidized during calcination. However, the complete conversion of AMO to pyrolusite does not occur after 4 h of calcination at 400°C, as several cryptomelane peaks are still observed.

The precipitation of AMO on γ-Al_2O_3 leads to the formation of a light-brown material. Unlike AMO, this material does not crystallize after 4 h of calcination at 400°C. The XRD pattern shown in Fig. 4 indicates that the manganese oxide phase is amorphous. The two peaks seen at 2.39 and 1.96 Å are due to the γ-Al_2O_3 support. While we have not measured the average Mn oxidation state in this material, the light-brown color seems to suggest that a considerable amount of Mn may be present in a lower oxidation state, perhaps as Mn^{3+}. We are currently examining this material by X-ray photoelectron spectroscopy to assist in determining the average Mn oxidation state.

Mn/Al_2O_3, prepared by wet impregnation of manganese(II) nitrate, leads to a black material, which after calcination at 400°C forms a crystalline material as seen in the XRD pattern in Fig. 5. Besides the peak at 1.97 Å (which is due to γ-Al_2O_3), the other peaks can all be assigned to pyrolusite. The XRD data correlate to the black color, which is common in MnO_2 materials.

B. Catalytic data. The data of Fig. 6 indicate that DMMP is decomposed over AMO to form CO_2 and MeOH. At 200°C, only a small amount of reaction occurs as the protection time is a few minutes. As the temperature is increased to 300 and 400°C, a significant increase in the amount of DMMP decomposition is observed. The formation of CO_2 toward the beginning of the reaction suggests that DMMP is completely oxidized. After approximately an hour, a steadily increasing amount of MeOH and DMMP appears in the gas stream, while the CO_2 concentration begins to decrease. This suggests that the catalyst surface is being poisoned and that the oxidation mechanism shuts off while a hydrolysis mechanism begins to dominate. Such trends are frequently observed for DMMP decomposition reactions over metal oxides (2, 11, 14).

The poisoning of catalyst surfaces by PO_x species is common in catalytic oxidation studies of DMMP. The total oxidation of DMMP can be represented by (14)

$$CH_3(CH_3O)_2PO + (x+15)/2O_2 \rightarrow 3CO_2 + 3/2H_2O + PO_x. \quad [1]$$

The PO_x species can combine with H_2O to form H_3PO_4, which contributes to catalyst poisoning. It is usually very difficult to remove PO_x species in the gas phase. For example, Lee *et al.* observed that, even at temperatures as high as 500°C, phosphorous compounds could not be removed from the surface of Cu-substituted hydroxyapatite catalysts (14).

The data of Fig. 7 indicate that the DMMP decomposition reaction is affected by changes made in the experimental conditions. The increase in flow rate from 30 to 50 mL/min causes a decrease in the rate of reaction. This is probably due to the increase in residence time within the reactor. With regard to the catalyst amount, one might expect that doubling the catalyst amount would cause an increase in the DMMP decomposition rate. However, it appears that any increase in the DMMP decomposition rate caused by increasing the amount of catalyst is offset by use of the higher flow rate.

In comparison to data obtained in our previous investigations concerning photo-assisted DMMP decomposition reactions, the thermal activation of DMMP is much

more effective. In that work we observed considerable adsorption of DMMP to the AMO surface under dark conditions (at Room T), with small amounts of MeOH also being produced (2). When the sample was irradiated with UV-vis light, an initial burst of product formation (CO_2 and MeOH) was observed. This activity lasted for only several minutes, with the catalyst quickly deactivating due to poisoning. In addition, we observed no PO_4^{3-} on the surface of AMO after photoreactions, which indicated the incomplete decomposition of DMMP (2).

The DMMP decomposition data for γ-Al_2O_3 in Fig. 8a indicate that the support itself is very active in decomposing DMMP, as a protection time of 15 h is observed. The long protection time may be due to the large surface area (291 m^2/g) of the support. However, the mechanism for DMMP decomposition using γ-Al_2O_3 appears to be different than that observed for AMO catalysts. The major difference is that when using γ-Al_2O_3 as a catalyst, no CO_2 is produced. This makes sense since no redox active metal is present. Therefore, DMMP is not oxidized over γ-Al_2O_3.

Another observation is that dimethyl ether is produced, especially toward the beginning of the reaction. The formation of DME is probably caused by the dehydration of MeOH by the Al_2O_3 surface. DME has been observed as the major product in MeOH oxidation reactions over γ-Al_2O_3 at temperatures up to 225°C (22). It appears that once the catalyst becomes saturated with P-species (marked by the appearance of DMMP and MeOH in the gas phase), the Al_2O_3 surface is no longer able to dehydrate MeOH and therefore MeOH begins to appear in the gas stream. The formation of DME and MeOH over γ-Al_2O_3 is similar to results obtained in the destructive adsorption of DMMP over MgO (7–9).

The catalytic results for DMMP decomposition over the two Al_2O_3-supported manganese oxide samples shown in Figs. 8B and 8C indicate protection times which are intermediate between that observed using AMO and the bare support. In both samples, CO_2 is observed, indicating that DMMP is oxidized. Similar to results obtained using AMO, after several hours the CO_2 levels decrease and the MeOH concentration increases. From these data it is clear that the use of the high surface area support aids in increasing the amount of DMMP decomposition (compared with unsupported AMO). The protection time for AMO/Al_2O_3 is almost twice that of the Mn/Al_2O_3 catalyst. We are not sure why this longer protection time occurs with AMO/Al_2O_3. However, it appears that this may be due to differences in the nature of the manganese species. Perhaps differences in the manganese oxidation state, dispersion, and surface area contribute to the differences in the catalytic data. We are currently using BET methods to examine the catalysts' surface areas to assist in explaining these trends. The XRD data for AMO/Al_2O_3 indicate that the MnO_x phase is amorphous. This may suggest that the crystallite size is too small to be detected by XRD indicating highly dispersed and high surface area MnO_x.

C. IR, IC analyses and mechanism. The IR data for AMO indicate that fresh AMO has a broad peak at 3300 cm^{-1} and a smaller peak at 1622 cm^{-1}, which are due to O–H vibrations. The broad peak at 500 cm^{-1} is caused by Mn–O vibrations. After DMMP reaction, the peaks due to O–H vibrations decrease significantly, suggesting that DMMP reacts with surface hydroxyl groups. The new peaks that appear in the lower portion of the spectrum (below 1800 cm^{-1}) indicate the presence of adsorbed phosphorous species. The peak at 1250 cm^{-1} is caused by the P=O vibration. Since the peak is shifted toward a weaker energy (compared with liquid DMMP), this suggests that the P=O moiety is involved in the bonding to the AMO surface. In photo-assisted DMMP decomposition reactions over AMO we observed similar trends (2). The interaction of P=O with Mn is consistent with a Lewis acid/base type adsorption mechanism. The phosphoryl oxygen is electron-rich (16) and can act as a Lewis base, which can interact with Lewis acid sites on AMO (i.e., Mn^{3+}, Mn^{4+}). This leads to the formation of Mn–O=P bonds, which likely weaken the P=O bonds, consistent with the IR data.

The other bands observed at 1238, 1088, 1029, 925, and 711 cm^{-1} are due to P–C vibrations, methyl deformations, and different types of P–O vibrations. While the IR data indicate the presence of P–CH_3, it appears as if initially, (during the protection time) P–CH_3 is oxidized. This seems likely because of IC data, which indicate the formation of PO_4^{3-} on the catalyst surface. This could be produced only if DMMP is completely oxidized. Perhaps once the surface is saturated with PO_4^{3-}, the surface becomes poisoned and additional DMMP is no longer oxidized.

The production of MeOH is indicative of a hydrolysis mechanism. Most likely, hydrolysis of the methoxy groups occurs by abstraction of a hydrogen from the surface hydroxyls, which then evolves as MeOH. Since no C–O vibrations are observed under these conditions, this suggests that at 400°C all methoxy groups are lost. This is consistent with results observed for many metal oxides in the literature (10, 11, 14). Another observation is that the bands in the higher frequency portion of the IR spectrum (3200–2600 cm^{-1}) are absent. Therefore, the decomposition mechanism over AMO is similar to that observed in photo-assisted decomposition reactions, except that here the reaction proceeds further with loss of all methoxy groups to oxidation to CO_2.

The IR data for γ-Al_2O_3 indicate that the fresh support has a strong, broad peak centered at 3470 cm^{-1}, which is due to O–H vibrations. The peaks at 1636, 1540, and 1368 are also due to O–H vibrations. These peaks disappear after reaction with DMMP, which indicates that they react with DMMP. Broad peaks centered at 762 and 570 cm^{-1} are due to Al–O vibrations. The IR spectrum of Al_2O_3 after DMMP

reactions indicates the formation of several new peaks in both the lower and the higher frequency regions. Since the P=O stretch is shifted by almost 100 cm^{-1} to 1165 cm^{-1}, this suggests that DMMP interacts very strongly with Al_2O_3 and that the bond is weakened considerably. As with AMO catalysts, the peaks at 1321, 1108, 918, and 802 cm^{-1} indicate the presence of P–C, P–O, and C–H bonds. Again, since no C–O peaks are observed, this suggests that all of the methoxy groups are lost.

Unlike AMO, a few peaks are observed in the higher frequency region of the spectrum. These include peaks at 3001 and 2935 cm^{-1}, which are due to methyl stretches in the PCH_3 group. Since no methyl stretches were observed for OCH_3 groups, further evidence is provided that all methoxy groups are lost during the reaction. The reason why the high frequency peaks are observed with γ-Al_2O_3 and not with AMO may be due to the fact that the reaction was run for a longer time (23 vs 6.5 h) and that γ-Al_2O_3 has a higher surface area, leading to a higher concentration of adsorbed species. No CO_2 was observed to form in the gas phase during reactions. However, the IC data do indicate the presence of small amounts of PO_4^{3-}. We are not sure why this happens. The major product observed on Al_2O_3 after thermal DMMP decomposition reactions is MPA. These results are consistent with data in the literature, whereby DMMP is not oxidized over Al_2O_3; rather it dissociatively adsorbs on Al_2O_3, with loss of both methoxy groups (at 400°C) to form adsorbed MPA (10, 16).

The IR spectra for the AMO/Al_2O_3 and Mn/Al_2O_3 catalysts exhibit similar trends to that observed using AMO. After reaction with DMMP, both samples show a similar shift in the P=O stretch toward lower energies. Similar peaks are observed in the P–C, P–O, and methyl deformation regions of the lower frequency portion of the spectra. Also, no C–O peaks are observed. These results suggest that a similar mechanism of DMMP decomposition occurs using Al_2O_3-supported manganese oxide catalysts as with AMO. The main difference is the use of Al_2O_3 causes an increase in the protection time, which is attributable to the higher surface area and increased dispersion of the redox active manganese.

The turnover numbers shown in Table 4 indicate that the thermal decomposition of DMMP over AMO (400°C) is several orders of magnitude greater than TONs for photoreactions. The most active catalysts are the manganese-oxide-supported Al_2O_3 materials. Both of these catalysts result in TONs greater than 1, suggesting that the reaction occurs catalytically over these materials. Al_2O_3 appears to be a good support for DMMP decomposition reactions due to its: (a) reactivity toward DMMP, (b) high surface area, and (c) good dispersion of manganese. There also appears to be a synergistic effect in DMMP decomposition activity by supporting manganese oxide on Al_2O_3, as TONs for Al_2O_3 (0.0458) and AMO (0.179) do not add up to values obtained for TONs of supported manganese oxide catalysts (1.22 and 1.87).

V. CONCLUSIONS

DMMP is thermally decomposed over AMO in the presence of air to form CO_2 and MeOH in the gas phase and MMP, MPA, and PO_4^{3-} on the catalyst surface. The temperature is the key parameter in affecting the rate of reaction. The highest rates were obtained at 400°C. Turnover numbers for thermal DMMP decomposition reactions over AMO at 400°C were several orders of magnitude greater than turnover numbers for photo-assisted reactions. The rates of thermal decomposition reactions were also found to be dependent on catalyst amount and reactant flow rates. The mechanism of thermal decomposition over AMO occurs similarly to that in photo-assisted reactions, except that at the temperatures used in these experiments all methoxy groups are lost, presumably to oxidation to CO_2. The presence of PO_4^{3-} on the AMO surface after reaction at 400°C indicates the complete oxidation of DMMP (P–CH_3 oxidation), especially during the protection time. After several hours, the catalyst becomes poisoned, and hydrolysis of DMMP occurs (formation of MeOH).

Both Al_2O_3 and Al_2O_3-supported manganese oxides are active materials for thermal DMMP decomposition reactions. The bare support had the longest protection time of all catalysts. Major products formed over Al_2O_3 included DME and MeOH. No CO_2 was produced when using Al_2O_3, indicating that DMMP is not oxidized. The mechanism of decomposition over Al_2O_3 appears to occur by dissociative adsorption of DMMP.

The most active catalysts for DMMP decomposition reactions were those prepared by supporting manganese oxide on Al_2O_3, especially by precipitation of AMO onto Al_2O_3. Turnover numbers for reactions over these materials were the highest (>1), suggesting that the reaction proceeds catalytically. Mechanistically, the reactions appear to occur similarly to those performed over AMO. However, poisoning by phosphorous species still occurs with these materials, leading to reduced DMMP decomposition activity. The poisoning of solid catalysts by phosphorous-containing species continues to be problematic and remains a challenge for future work in catalytic decomposition studies of chemical warfare agents.

It may be interesting to see what effects adding vanadium to either manganese oxide or supported manganese oxide materials has on the DMMP decomposition activity. Recent results from our lab clearly indicate the superiority of V_xO_y supported on Al_2O_3 and SiO_2 for DMMP decomposition as protection times >100 h were observed at 450°C (15). Additionally, the use of higher temperatures (>500°C) in DMMP decomposition studies may be beneficial for the

formation of gaseous P-species species which could prolong the activity of the manganese oxide catalysts.

ACKNOWLEDGMENTS

We thank the U.S. Army and United Technologies Research Center (East Hartford, CT) for this work. This work was supported by the U.S. Army Research Office, under Contract DAAH04-96-C-0067.

REFERENCES

1. Obee, T. N., and Satyapal, S., *J. Photochem. Photobiol A Chem.* **118**, 45–51 ((1998).
2. Segal, S. R., Suib, S. L., Tang, X., and Satyapal, S., *Chem. Mater.* **11**, 1687–1695 (1999).
3. Smentkowski, V. S., Hagans, P., and Yates, J. T., *J. Phys. Chem.* **92**, 6351–6357 (1988).
4. Henderson, M. A., and White, J. M., *J. Am. Chem. Soc.* **110**, 6939–6842 (1988).
5. Guo, X., Yoshinobu, J., and Yates, J. T., *J. Phys. Chem.* **94**, 6839–6842 (1990).
6. Hedge, R. I., and White, J. M., *Appl. Surf. Sci.* **28**, 1–10 (1987).
7. Li, Y. X., and Klabunde, K. J., *Langmuir* **7**, 1388–1393 (1991).
8. Li, Y. X., Koper, O., Atteya, M., and Klabunde, K. J., *Chem. Mater.* **4**, 323–330 (1992).
9. Lin, S. T., and Klabunde, K. J., *Langmuir* **1**, 600–605 (1985).
10. Mitchell, M. B., Sheinker, V. N., and Mintz, E. A., *J. Phys. Chem. B* **101**, 11192–11203 (1997).
11. Tzou, T. Z., and Weller, S. W., *J. Catal.* **146**, 370–374 (1994).
12. Tesfai, T. M., Sheinker, V. N., and Mitchell, M. B., *J. Phys. Chem. B* **102**, 7299–7302 (1998).
13. Jiang, Y., Decker, S., Mohs, C., and Klabunde, K. J., *J. Catal.* **180**, 24–35 (1998).
14. Lee, K. W., Houalla, M., Hercules, D. M., and Hall, W. K., *J. Catal.* **145**, 223–231 (1994).
15. Cao, L., Segal, S. R., Suib, S. L., Tang, X., and Satyapal, S., *J. Catal.* **194**, 61–70 (2000).
16. Templeton, M. K., and Weinberg, W. H., *J. Am. Chem. Soc.* **107**, 97–108 (1985).
17. Christol, H., Levy, M., and Marty, C., *J. Org. Chem.* **12**, 459–470 (1968).
18. Chen, J., Lin, J. C., Purohit, V., Cutlip, M. B., and Suib, S. L., *Catal. Today* **33**, 205–214 (1997).
19. Kapteijn, F., Singoredjo, L., Andreini, A., and Moulijn, J. A., *Appl. Catal. B Environ.* **3**, 173–189 (1994).
20. Lin, J. C., Chen, J., Suib, S. L., Cutlip, M. B., and Frehaut, J. D., *J. Catal.* **161**, 659–666 (1996).
21. Segal, S. R., Suib, S. L., and Foland, L., *Chem. Mater.* **9**, 2526–2532 (1997).
22. Ozkan, U. S., Kueller, R. F., and Moctezuma, E., *Ind. Eng. Chem. Res.* **29**, 1136–1142 (1990).